NON-MAGNETIC ON-CHIP RESONANT ACOUSTO-OPTIC ISOLATOR AT 780 nm

Gaurav Bahl

University of Illinois
506 S. Wright St.
364 Henry Admin Bldg.
Urbana, IL 61801-3620

04 August 2017

Final Report

AIR FORCE RESEARCH LABORATORY
Space Vehicles Directorate
3550 Aberdeen Ave SE
AIR FORCE MATERIEL COMMAND
KIRTLAND AIR FORCE BASE, NM 87117-5776

DTIC COPY

NOTICE AND SIGNATURE PAGE

Using Government drawings, specifications, or other data included in this document for any purpose other than Government procurement does not in any way obligate the U.S. Government. The fact that the Government formulated or supplied the drawings, specifications, or other data does not license the holder or any other person or corporation; or convey any rights or permission to manufacture, use, or sell any patented invention that may relate to them.

This report is the result of contracted fundamental research which is exempt from public affairs security and policy review in accordance with AFI 61-201, paragraph 2.3.5.1. This report is available to the general public, including foreign nationals. Copies may be obtained from the Defense Technical Information Center (DTIC) (http://www.dtic.mil).

AFRL-RV-PS-TR-2017-0170 HAS BEEN REVIEWED AND IS APPROVED FOR PUBLICATION IN ACCORDANCE WITH ASSIGNED DISTRIBUTION STATEMENT.

//SIGNED//   //SIGNED//

_____   _____
Dr. Brian Kasch   Dr. Thomas R. Caudill, Acting Chief
Program Manager, AFRL/RVBYE   AFRL Battlespace Environment Division

This report is published in the interest of scientific and technical information exchange, and its publication does not constitute the Government's approval or disapproval of its ideas or findings.

REPORT DOCUMENTATION PAGE

1. REPORT DATE *(DD-MM-YYYY)* 04-08-2017	2. REPORT TYPE Final Report	3. DATES COVERED *(From - To)* 09 Nov 2015 – 01 Jul 2017
4. TITLE AND SUBTITLE Non-Magnetic On-Chip Resonant Acousto-Optic Isolator at 780 nm		5a. CONTRACT NUMBER FA9453-16-1-0025
		5b. GRANT NUMBER
		5c. PROGRAM ELEMENT NUMBER DoD, DARPA
6. AUTHOR(S) Gaurav Bahl		5d. PROJECT NUMBER DoD, DARPA
		5e. TASK NUMBER PPM00036053
		5f. WORK UNIT NUMBER EF129686
7. PERFORMING ORGANIZATION NAME(S) AND ADDRESS(ES) University of Illinois 506 S. Wright St. 364 Henry Admin Bldg. Urbana, IL 61801-3620		8. PERFORMING ORGANIZATION REPORT NUMBER
9. SPONSORING / MONITORING AGENCY NAME(S) AND ADDRESS(ES) Air Force Research Laboratory Space Vehicles Directorate 3550 Aberdeen Avenue SE Kirtland AFB, NM 87117-5776		10. SPONSOR/MONITOR'S ACRONYM(S) AFRL/RVBYE
		11. SPONSOR/MONITOR'S REPORT NUMBER(S) AFRL-RV-PS-TR-2017-0170

12. DISTRIBUTION / AVAILABILITY STATEMENT
Approved for public release; distribution is unlimited.

13. SUPPLEMENTARY NOTES

14. ABSTRACT
The goal of this project was to demonstrate a lithographically defined proof-of-concept optical isolator on-chip, without the use of magnetic fields or magneto-optical materials. Our technical approach was to employ momentum-conservation in photon-phonon interactions to break the propagation symmetry of light using a unidirectional acoustic pump. This acoustic wave was transduced using an RF-driven SAW actuator on a piezoelectric substrate. We fabricated the device using only CMOS-compatible dielectric materials with the assistance of e-beam lithopgraphy. The final device operated as a frequency-shifting isolator near 1550 nm (telecom wavelength) and exhibited 15 dB of non-reciprocal contrast with 7.7 dB insertion loss. We also demonstrated on-chip components that would permit implementation of this isolator at 780 nm for cold-atom microsystems applications, laying out paths for future development and improvements.

15. SUBJECT TERMS
optical isolator, acousto-optics, non-reciprocal devices, nonlinear optics, aluminum nitride, single-sideband modulation, interband scattering, momentum conservation, optomechanics, optical circulator

16. SECURITY CLASSIFICATION OF:			17. LIMITATION OF ABSTRACT	18. NUMBER OF PAGES	19a. NAME OF RESPONSIBLE PERSON Dr. Brian Kasch
a. REPORT Unclassified	b. ABSTRACT Unclassified	c. THIS PAGE Unclassified	Unlimited	22	19b. TELEPHONE NUMBER *(include area code)*

This page is intentionally left blank.

Table of Contents

List of Figures

ACKNOWLEDGMENTS

DISCLAIMER

The views and conclusions contained herein are those of the authors and should not be interpreted as necessarily representing the official policies or endorsements, either expressed or implied, of Air Force Research Laboratory or the U.S. Government.

This page is intentionally left blank.

1.   Introduction

Non-reciprocal devices (e.g. isolators and circulators), in which time reversal symmetry is broken for light propagation, provide critical functionalities for signal routing and source protection in photonic systems. The most commonly encountered non-reciprocal devices are isolators and circulators, which are typically manufactured today using magneto-optic techniques. However, for cold atom microsystems (e.g. inertial sensors, clocks) magnetic fields are extremely undesirable as they can produce Zeeman shifts and light shifts resulting in inaccurate measurements. Adequate magnetic shielding can be very challenging to produce at small size scales, which prohibits sensor miniaturization. Additionally, the optical losses in magneto-optical isolators that operate at 780 nm (for Rb) and 854 nm (for Cs) wavelengths can be very challenging to overcome. Thus, a new approach is desired.

In this context, optomechanical devices [1] with non-reciprocal properties offer a unique opportunity to produce isolators and circulators, without needing materials having optical gain or magneto-optical activity. Additionally, such devices can be produced using nearly any transparent dielectric material and can thus achieve extremely small insertion loss. Prior to the initiation of our project, however, all non-reciprocal optomechanical devices only operated over kHz-MHz bandwidth rendering them impractical. In this report, we present our new approach for obtaining non-reciprocal optomechanical devices having GHz-regime bandwidths and large optical contrast. We achieved this by inverting the roles of the mechanical and optical modes in a common optomechanical configuration so that acoustic excitation can be used to break time-reversal symmetry (driven by RF input). The transformative implications of our results are that we no longer need additional lasers to drive the non-reciprocal effect, and the linearity of the effect is not limited to small optical signals.

As the final result of this project, we have implemented a non-reciprocal frequency-shifting nanophotonic isolator near 1550 nm (telecom) wavelength. Light entering the device is transferred to a second optical mode through phonon-mediated indirect interband scattering [2-4] i.e. a single-sideband modulation effect is obtained. Light entering from the opposite direction is simply resonantly absorbed. The completed device was shown to operate as a frequency shifting isolator and produced 15 dB optical contrast with up to 17% mode conversion efficiency (i.e. 7.7 dB forward insertion loss). This report describes the architecture, fabrication, operation, and key measurements on the device, and identifies paths forward to achieving linear optical isolation at 780 nm.

2.   Background

Presently, vital non-reciprocal optical devices are exclusively built using magneto-optic interactions [5-8]. This mechanism, called the Faraday effect, requires materials that offer a strong magnetically induced direction-asymmetric polarization rotation (e.g. garnets). By employing suitable polarization filters or birefringent filters, light propagating in the forward direction can be transmitted, while strongly attenuating light in the backward direction. However the on-chip integration of requisite materials (garnets and magnets) is costly, requires special materials processing [8-15], and imposes wavelength restrictions. Thus, the technique is not suited for

implementation in photonics foundries, and is not readily adapted to desired wavelengths. Alternative techniques for optical isolation have involved the use of spatio-temporal modulation and nonlinearities. The most recent experimental attempt at using RF-modulation (to achieve interband scattering) showed only 3 dB of optical isolation with a very large ~25 dBm RF power cost and >70 dB insertion loss [16,17]. Other theoretical approaches include angular momentum biasing [18,19], opto-mechanical effects [20,21], electro-optic inter-band transitions [3,16], acousto-optic scattering [9,11], and helicity sensitive transitions in quantum dots [5-8,22]. Isolation through Brillouin interband transitions has been proposed before [8-10,12-15] in highly nonlinear fiber systems, but is challenging to implement on-chip [11,16,17] due to low efficiency, and high power and device length requirements. Our recent work on non-reciprocal acousto-optical scattering in microresonators [23] generated key insights that have enabled this project. Our results overcome the key technical challenges that have persisted in previous work [16,17,20,21]; specifically with regards to poor RF-power efficiency and poor isolation contrast.

3.　　Developed concept – Achieving non-reciprocal optical scattering with phonons

Consider a racetrack optical resonator supporting TE_{10} (ω_1, k_1) and TE_{00} (ω_2, k_2) optical modes as illustrated in Fig. 1a. Indirect intermodal scattering [3] is defined as the transfer of photons between two modes having unequal momentum and unequal frequency, and can be enabled in this resonator by the photoelastic perturbations (e.g. change in refractive index by strain) created by an acoustic wave having frequency $\Omega = \omega_2 - \omega_1$ and momentum $q = k_2 - k_1$ [24,25]. The phase-matching condition for this interaction is visually presented in Fig. 1b. It can be seen that excitation of the resonator with phonons having (Ω, q) enables acousto-optical scattering for backward propagating optical signals only (in this example). Light in the opposite direction (forward, in this example) does not see the correct phase-matching and simply is absorbed by the optical resonator. This directional asymmetry for interband scattering implies that the system has broken time-reversal symmetry.

　　　　It is also important to recognize that to achieve interband scattering, the phonon mode must assist with breaking the orthogonality between the optical modes of the resonator. Fig. 2 conveys the implication of the above statement. Since the mode shapes (transverse electric field) of the TE_{10} and TE_{00} resonator modes are odd and even, respectively, the density variation from the acoustic wave must also be odd in order to break orthogonality. We have discussed the orthogonality condition in more detail in our supporting manuscript [26].
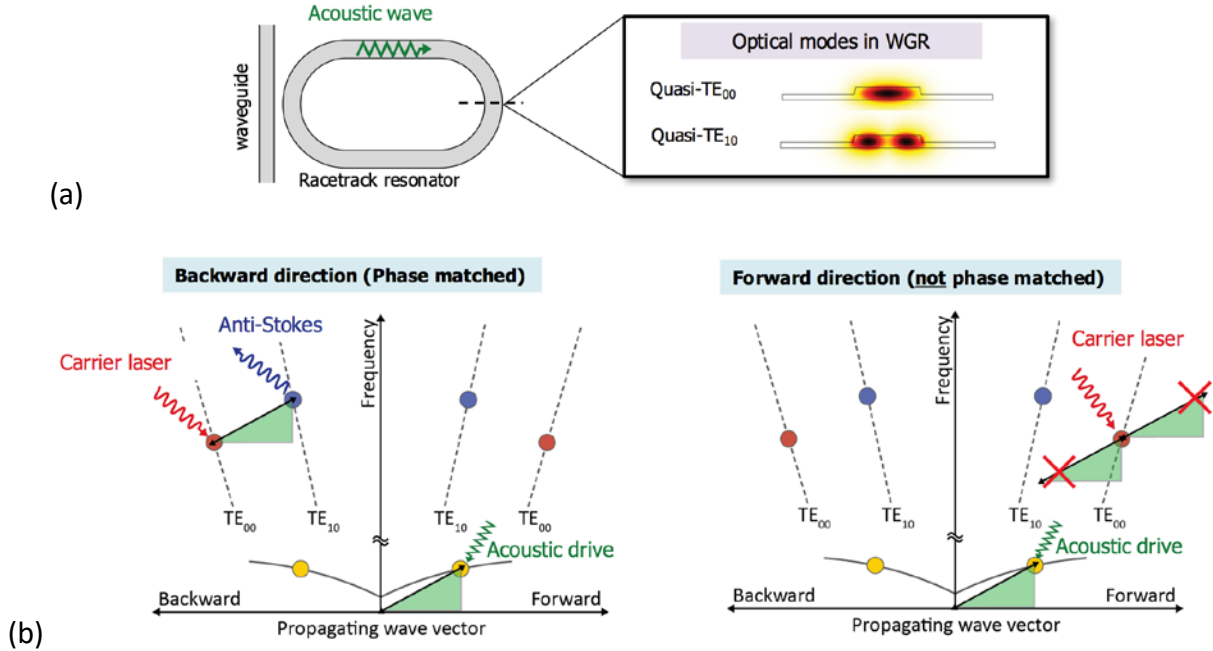
(a)

(b)

Fig 1: (a) Illustration of our racetrack resonator design for the nonreciprocal modulator, and the supported optical modes. (b) Phase-matching diagrams for forward and backward propagating optical signals ("carrier") through the non-reciprocal modulator. *In the backward direction, the optical carrier is mode-converted and an anti-Stokes single sideband is generated. In the forward direction the light is simply absorbed by the device. Figure adapted from our manuscript* [26].
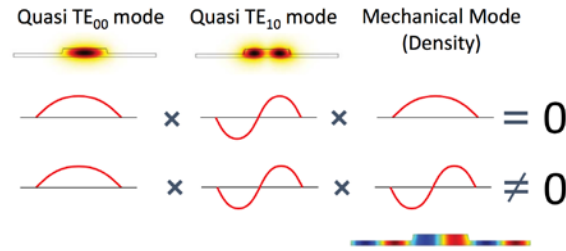

Fig 2: Cross-sectional shape selection for the mechanical mode, given the two optical mode shapes. *We concluded that to obtain non-zero scattering, the mechanical mode density must also have odd transverse shape.*

In order to produce an experimental system supporting the above physics, we require an interdigitated transducer (IDT) that can launch an acoustic wave with the correct momentum, frequency, and transverse shape parameters to enable interband scattering. Our design concept is shown in Fig. 3. For our specific experimental non-reciprocal modulator, we determined first that an acoustic momentum (propagation constant) of $q_{propagating}$ = 3.54×10^5 m^{-1} would be required to match the propagating momentum difference of the two optical modes. An acoustic free edge reflector (AlN device layer was etched through to the air below) was placed at 2 acoustic wavelegnths away from the waveguide center for obtaining an odd

acoustic density profile within the waveguide. For maximizing the optomechanical overlap integral, the transverse propagation constant was set to $q_{transverse} = 2\pi/2.2 \ \mu m^{-1} = 2.86 \times 10^6 \ m^{-1}$. To obtain the correct momenta simultaneously, the IDT angle was set to $\theta = \tan^{-1}(q_{propagating}/q_{transverse}) = 7.06°$, and electrode pitch was set to $\Lambda = \pi/2q_{total} = 546$ nm. An electronic stimulus of 4.82 GHz was needed to drive an S_0 Lamb surface acoustic wave having the required propagation constants.
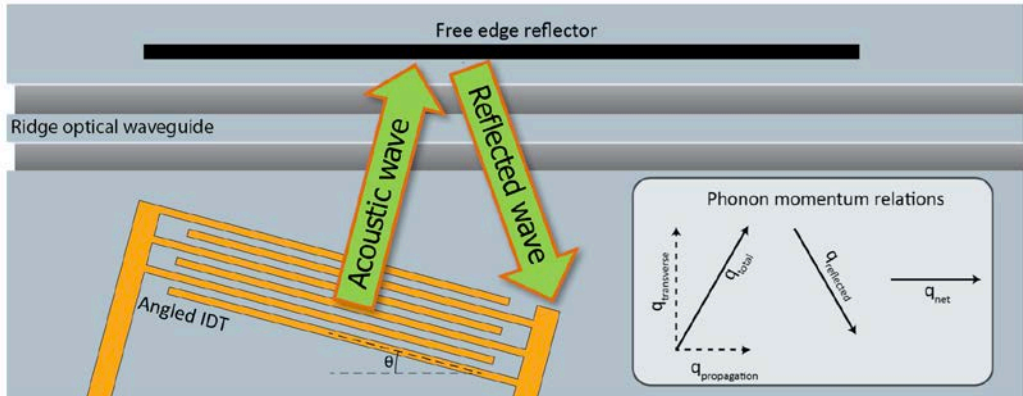

Fig 3: Schematic of the IDT system designed to drive the acoustic wave through an optical waveguide. *We selected the IDT pitch and angle to simultaneously achieve all required physical parameters for the acoustic wave. Figure adapted from our manuscript* [26]*.*

4.   Device fabrication

We fabricated the non-reciprocal frequency-shifting isolator on an aluminum nitride (AlN) device layer on air platform, having an underlying silicon handle wafer. AlN was selected since it has very low loss in the telecom band (1550 nm) and also in the frequency bands commonly used for cold atoms systems (780 nm, 854 nm). AlN is also an excellent acoustic material on which phonons can be driven via piezoelectric drive through an electronic stimulus. 350 nm of c-axis oriented AlN was obtained by RF sputtering onto a silicon wafer. The devices were then patterned through three electron-beam lithography steps. The AlN waveguide and racetrack resonator were first patterned on e-beam resist. Then, 200 nm of AlN was etched back using Cl_2 inductively coupled plasma reactive ion etching (ICP-RIE) to define the racetrack waveguide and resonator system along with the optical grating couplers. Next, the release holes and edge reflector were patterned also using e-beam lithography on double spin coated e-beam resist, followed by complete etch of the 350 nm AlN down to air below via ICP-RIE. Finally, the IDT was patterned with e-beam lithography on PMMA photoresist and 60 nm of Al electrodes were evaporated to define the electrodes. A gas-phase etch was performed using XeF_2 to undercut the silicon and release the mechanical components. Images of the completed device are presented in Fig 4.
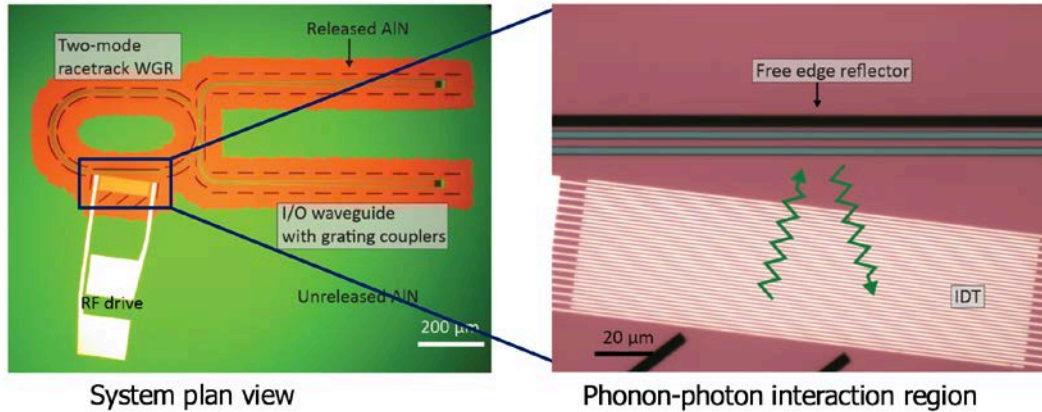
Fig 4: Microscope images of the completed non-reciprocal optical modulator.

5. Demonstration of non-reciprocal isolation (frequency-shifting isolator)

We performed measurements on the non-reciprocal optical modulator using the following experimental setup. We used a tunable telecom band external cavity diode laser to measure the optical propagation through the resonator-waveguide system via the waveguide grating couplers (Fig 4 - left). An optical switch controlled the direction in which the resonator was probed so that both forward and backward optical propagation could be tested. An erbium-doped fiber amplifier amplified the output optical signals to improve measurement. The optical carrier frequency and the optical sidebands were all monitored during the experiment, for various optical probe frequencies.

Results from our experiments are presented in Fig 5. The carrier laser entering the waveguide experienced resonant absorption dips corresponding to both resonator modes as shown in the data. When the IDT transducer was driven with 4.8 GHz RF signal, the acoustic waves enabled the indirect intermodal scattering only for backward propagating optical signals. Evidence for this is presented in the measured data, which shows that optical sidebands were only produced due to this scattering effect when the optical signal was propagating in the backward direction. For forward propagating signals, the optical sidebands were 15 dB smaller than the opposite case. This 15 dB of optical contrast was observed at the peak of the optical resonances, and the -3 dB bandwidth of the isolator system was approximately 1.1 GHz.

The insertion loss in such a frequency shifting modulator can be defined as the sideband conversion efficiency. In other words, how much optical power is converted from the carrier signal to the sideband without being lost? In our device this insertion loss improves with increased RF drive power since more light is converted to the second optical mode without being absorbed. As shown in Fig 6, the highest conversion efficiency of 17% was measured with 17.8 dBm RF drive power delivered to the IDT. At this point, we estimate an optomechanical coupling rate of 0.609 GHz. At higher RF drive power the device electrodes were damaged due to resistive heating.
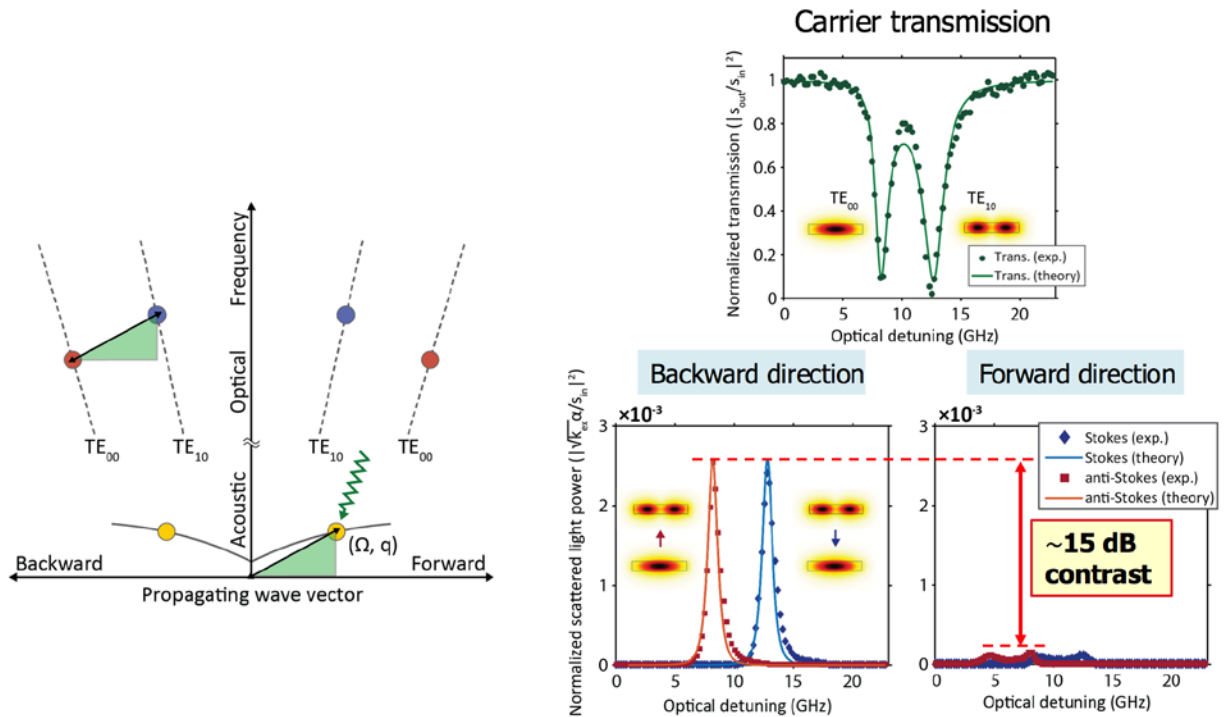
Fig 5: (Left) Phase matching situation in the experiment. (Right) Demonstration of non-reciprocal modulation i.e. single sideband scattering under RF drive power of 0 dBm, as a function of laser frequency (detuning). *The data shows a strong asymmetry in mode conversion between forward and backward propagating optical signals.*
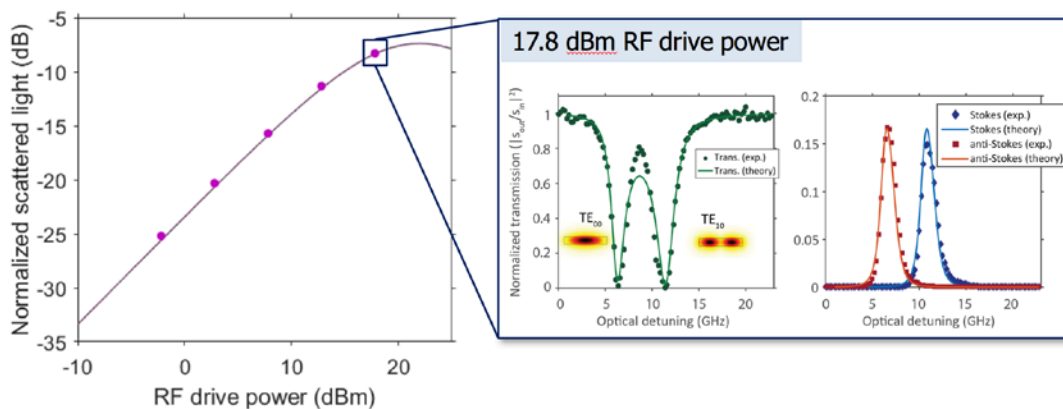

Fig 6: The highest mode conversion efficiency (percentage of light scattered, or insertion loss) reached its highest value of 17% at 17.8 dBm RF drive power.

6.   Outlook for future experiments I – Optical isolator operational regimes

Our non-reciprocal modulator can be designed to operate in two distinct regimes for obtaining optical isolation. Below, we discuss these regimes (more details are available in our manuscript [26]).

6a. Frequency-shifting isolator regime

The device that we have demonstrated operates as a frequency shifting isolator (Fig 7) – light passes through the device with a known frequency shift in the transmission direction, while in the opposite direction light is simply absorbed. This regime is achieved by our system for low RF drive power i.e. low optomechanical coupling.
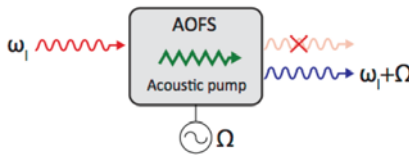

Fig 7: Concept of a frequency shifting optical isolator. The input laser appears at the output with a frequency shift, while in the opposite direction it is absorbed. Figure adapted from our manuscript [26].

6b. Linear optical isolator regime

If much stronger optomechanical coupling is achieved, then the scattering of light between the two optical modes creates a normal-mode splitting phenomenon. In this situation the device is transparent in the forward direction, and for infinite optomechanical coupling all the input optical power is sent to the output port. Due to the momentum conserving nature of the interaction this mode split only occurs in the direction in which the interaction is phase matched, i.e. is selected by the acoustic pump direction. Thus, in the opposite direction, the optical mode remains unmodified and light is simply absorbed by the device. This situation is illustrated in Fig 8. In this regime, the device operates as a linear optical isolator, with near-ideal characteristics. In other words, the optomechanical coupling rate and the waveguide-resonator coupling rate can be designed to exhibit near-perfect transparency in the forward direction and near-perfect absorption in the backward direction.

As explained above, the highest optomechanical coupling rate that we experimentally demonstrated was 0.609 GHz. The plots in Fig 8 use the experimental parameters from our device, and predict that the linear isolator regime would be accessible if our optomechanical coupling rate approaches 3 GHz. We were unable to reach this level of optomechanical coupling in our experiments (due to device failure) but we do have a clear path forward. First, the IDTs can be redesigned for improved power handling and heat-sinking. Second, the mechanical mode can be made resonant, which easily provides a huge boost to the acoustic power within the device, thereby increasing the optomechanical coupling.
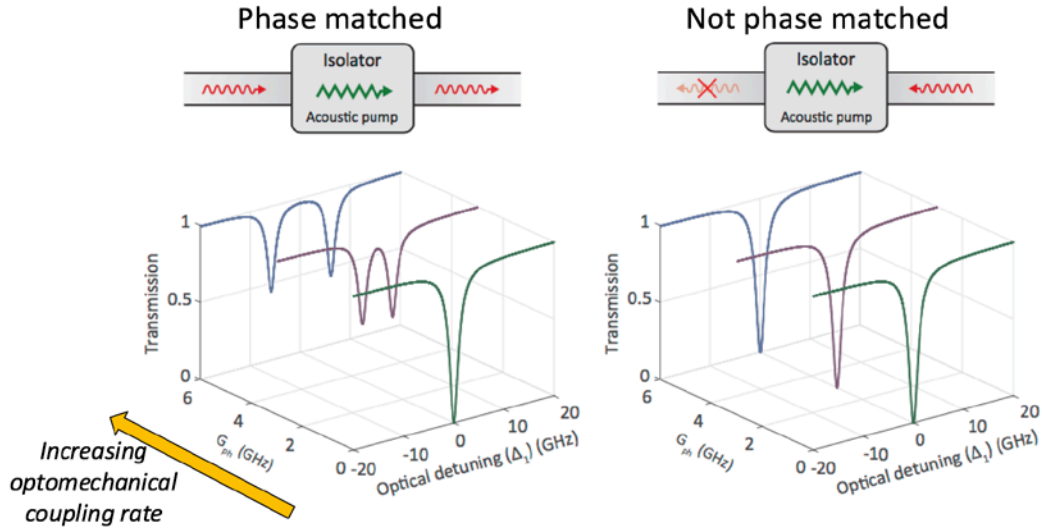
Fig 8: Our system will operate as a linear optical isolator at the center of the optical resonance if very large optomechanical coupling can be achieved. *Figure adapted from our manuscript* [26].

6c. Experimental confirmation

Experimental confirmation of our modeling of the isolator regimes is shown in Fig 9 – as the RF drive power increases, the amount of light scattering increases as well. However, at large RF drive (i.e. large optomechanical coupling), we will observe a normal mode split (Fig 8 - left) and a corresponding decrease in the amount of light modulation. This corresponds to the linear isolator regime, in which no light modulation takes place when infinite optomechanical coupling is made available.
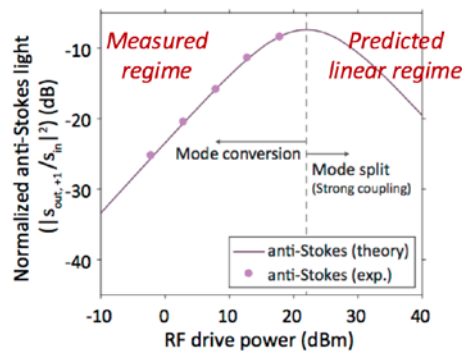

Fig 9: Dots correspond to measured data while the solid line corresponds to the predicted light scattering based on parameters directly measured from the experiment. *Prediction and experiment show very strong agreement. Figure adapted from our manuscript* [26].

7. Outlook for future experiments II – Demonstration of isolator at 780 nm

While our original goal was to demonstrate the RF-driven isolator system at 780 nm wavelength, we elected to pursue our initial proof-of-concept experiments at 1550 nm for technical convenience. However, we simultaneously produced all the essential components that would comprise this system at 780 nm wavelength. This includes optical racetrack resonators, grating couplers, and surface acoustic wave inter-digitated transducers. A plan view of the test system that we built is shown in Fig 10. Microscope images of these components are presented in Fig 11. Since our non-reciprocal system concept is well developed at 1550 nm wavelength, the path forward to implementation at 780 nm (or even 854 nm) is clearly laid out. Further pursuit of this isolator would require continued research support.
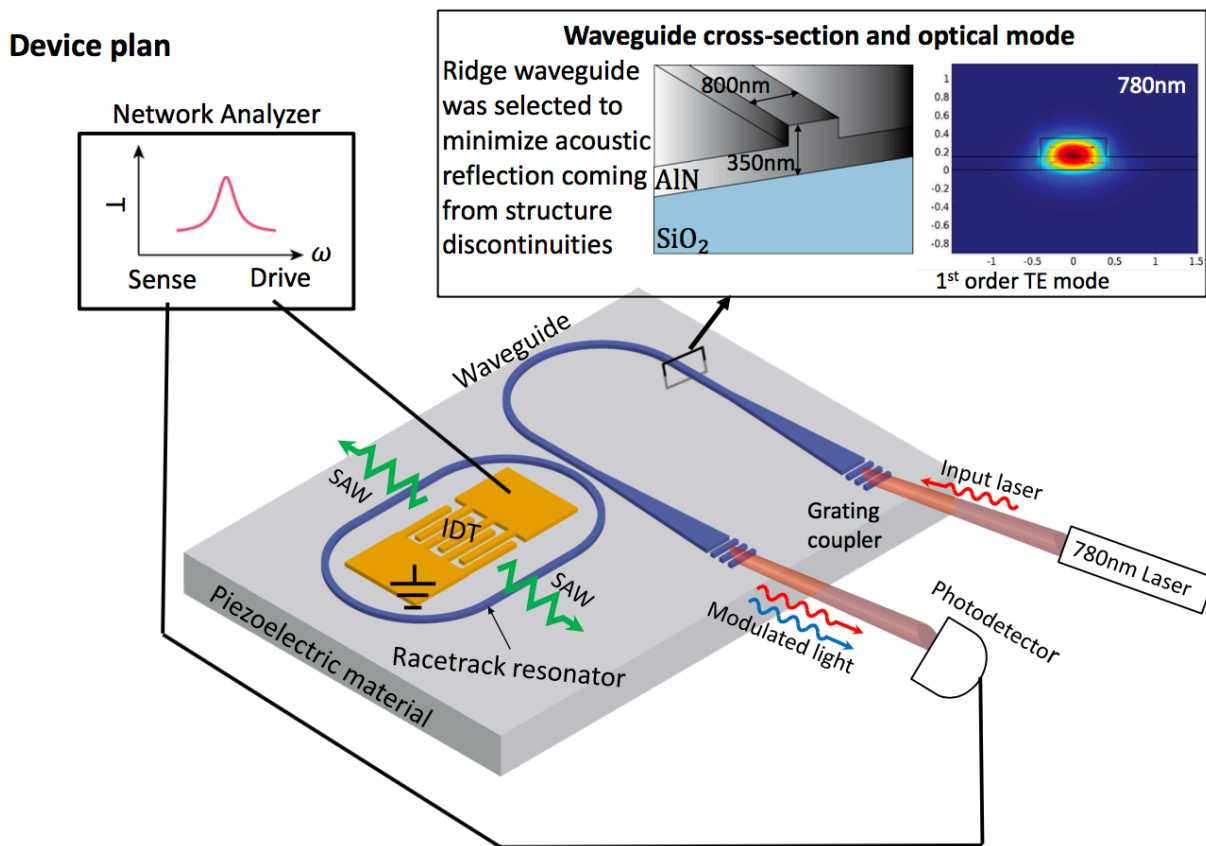

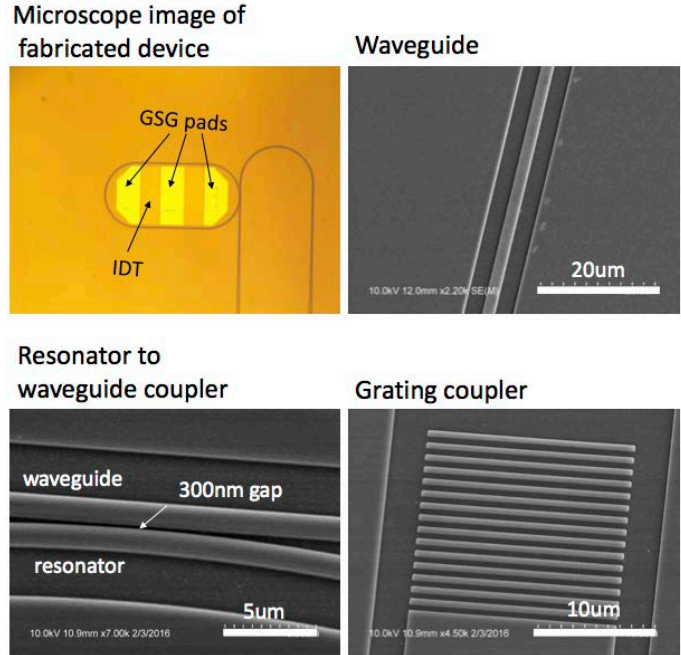**Fig 10: Schematic for 780 nm test system that we produced.**

Fig 11: Microscope images of resonator, IDT, waveguide, and couplers for 780 nm system.

8.   Conclusions

We have successfully demonstrated an on-chip frequency-shifting optical isolator (telecom wavelength) using common dielectric materials, that uses an RF stimulus to drive the non-reciprocal effect. Our system is produced using CMOS-compatible processes and materials that can be readily translated to photonics foundries. We have also successfully laid out paths towards to produce this isolator system at 780 nm wavelength, for applications in atom-based microsystems, and have identified a path for operating the device in the linear optical isolator regime. Our results will impact multiple DARPA programs on compact atomic timekeeping, cold-atom inertial navigation, and gravimetry. Since the entire system is lithographically defined, the optical isolation wavelength can be adapted according to the designer's needs. Our approach can also enable new non-reciprocal functions for chip-scale photonics including frequency shifting and mode division multiplexing.

References

1. Marquardt, F., *et al.*, *Cavity-Optomechanics Nano- and Micromechanical Resonators Interacting with Light,* Springer Berlin, 2015.
2. Kuhn, L., *et al.*, Optical Guided Wave Mode Conversion by an Acoustic Surface Wave, *Applied Physics Letters* **19,** pp. 428–430, 1971.
3. Yu, Z. and Fan, S., Complete optical isolation created by indirect interband photonic transitions, *Nature Photonics* **3,** p. 91, 2009.
4. Hwang, I. K., *et al.*, All-fiber-optic nonreciprocal modulator, *Optics Letters* **22,** pp. 507–509, 1997.
5. Aplet, L. J. and Carson, J. W., A Faraday Effect Optical Isolator, *Applied Optics* **3,** pp. 544–545, 1964.
6. Shirasaki, M. and Asama, K., Compact optical isolator for fibers using birefringent wedges, *Applied Optics* **21,** pp. 4296–4299, 1982.
7. Sato, T., *et al.*, Lens-free in-line optical isolators, *Optics Letters* **24,** pp. 1337–1339, 1999.
8. Dotsch, H., *et al.,* Applications of magneto-optical waveguides in integrated optics: review, *JOSA B* **22,** p. 240, 2005.
9. Kang, M. S., *et al.*, Reconfigurable light-driven opto-acoustic isolators in photonic crystal fibre, *Nature Photonics* **5,** pp. 549–553, 2011.
10. Stadler, B. J. H. and Gopinath, A., Magneto-optical garnet films made by reactive sputtering, *Magnetics, IEEE Transactions on* **36,** pp. 3957–3961, 2000.
11. Poulton, C. G., *et al.,* Design for broadband on-chip isolator using stimulated Brillouin scattering in dispersion-engineered chalcogenide waveguides, *Opt. Express* **20,** pp. 21235–21246, 2012.
12. Espinola, R. L., *et al.*, Magneto-optical nonreciprocal phase shift in garnet/silicon-on-insulator waveguides, *Optics Letters* **29,** p. 941, 2004.
13. Shoji, Y., *et al.*, Magneto-optical isolator with silicon waveguides fabricated by direct bonding, *Applied Physics Letters* **92,** pp. 071117–071117, 2008.
14. Tien, M.-C., *et al.*, Silicon ring isolators with bonded nonreciprocal magneto-optic garnets, *Optics Express* **19,** p. 11740, 2011.
15. Bi, L., *et al.,* On-chip optical isolation in monolithically integrated non-reciprocal optical resonators, *Nature Photonics* **5,** pp. 758–762, 2011.
16. Lira, H., *et al.*, Electrically Driven Nonreciprocity Induced by Interband Photonic Transition on a Silicon Chip, *Physical Review Letters* **109,** p. 033901, 2012.
17. Tzuang, L. D., *et al.*, Non-reciprocal phase shift induced by an effective magnetic flux for light, *Nature Photonics* **8,** pp. 701–705, 2014.
18. Sounas, D. L., *et al.*, Giant non-reciprocity at the subwavelength scale using angular momentum-biased metamaterials, *Nature Communications* **4**, 2013.
19. Sounas, D. L. and Alu, A., Angular-Momentum-Biased Nanorings To Realize Magnetic-Free Integrated Optical Isolation, *ACS Photonics* **1,** pp. 198–204, 2014.

20. Manipatruni, S., *et al.*, Optical Nonreciprocity in Optomechanical Structures, *Physical Review Letters* **102,** p. 213903, 2009.

21. Hafezi, M. and Rabl, P., Optomechanically induced non-reciprocity in microring resonators, *Optics Express* **20,** pp. 7672–7684, 2012.

22. Lenferink, E. J., *et al.*, Coherent optical non-reciprocity in axisymmetric resonators, *arXiv:*1404.4863, 2014.

23. Kim, J., *et al.*, Non-reciprocal Brillouin scattering induced transparency, *Nature Physics* **11,** pp. 275–280, 2015.

24. Bahl, G., *et al.*, Stimulated optomechanical excitation of surface acoustic waves in a microdevice, *Nature Communications* **2,** p. 403, 2011.

25. Bahl, G., *et al.*, Observation of spontaneous Brillouin cooling, *Nature Physics* **8,** pp. 203–207, 2012.

26. Sohn, D. B., *et al.*, Breaking time-reversal symmetry with acoustic pumping of nanophotonic circuits, *arXiv:1707.04276*[physics.optics], 2017.

DISTRIBUTION LIST

DTIC/OCP
8725 John J. Kingman Rd, Suite 0944
Ft Belvoir, VA 22060-6218   1 cy

AFRL/RVIL
Kirtland AFB, NM 87117-5776   1 cy

Official Record Copy
AFRL/RVBYE/Dr. Brian Kasch   1 cy

This page is intentionally left blank.